University of Groningen

MSc. Chemical Engineering
Internship Report

Annealing of 3D printed parts

Author:
Bart de Wijk

Supervisor:
dr. ir. Timon Rijnaarts

First Assessor:
dr. ir. Jingxiu Xie

Second Assessor:
prof. dr. Francesco Picchioni

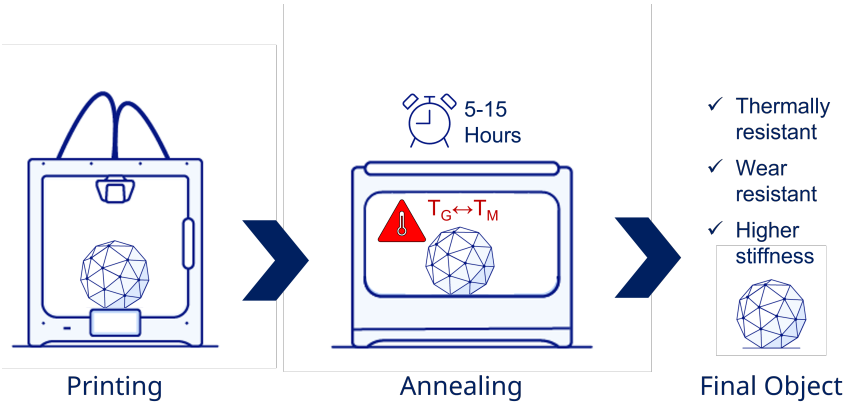

[.5cm]
February 25, 2022

Ultimaker

rijksuniversiteit groningen

Contents

1 Abstract

The effects of annealing on dimensional warping, mechanical properties and thermal resistance were evaluated for 3D-printed polylactic acid (PLA) and carbon-fiber-reinforced Polyethylene terephthalate (PET-CF). Various objects were printed using Fused Deposition Modeling (FDM) technology and tested for shrinkage, warping, Heat Deflection Temperature (HDT), flexural strength and modulus. Z-layer adhesion, characteristic for FDM and other 3D printing techniques, was also evaluated. PLA samples were annealed at 80 and 110 °C, PET-CF samples at 120, 170 and 220 °C. Lower annealing temperatures were associated with a higher flexural strength (18,5% for PET-CF), while higher annealing temperatures resulted in stiffer and more temperature resistant objects (modulus increase: 23,3%, HDT: 229 °C for PET-CF). Temperature resistance of PET-CF was more affected by annealing temperature than PLA. Shrinkage was limited across all annealing methods and materials ($\leq$ 1%) and dimensional warping was likewise a minimal issue when annealing below 220 °C. As a drawback, annealing resulted in significantly decreased Z-layer adhesion in all cases (flexural strength between -13 and -32% parallel to printed layers).

2 Introduction

The research presented in this document is the result of an internship conducted over four months at Ultimaker, a Dutch 3D-printer manufacturing company. Their printers are used worldwide in education and a wide variety of industries, including automotive, healthcare and architecture; functions range from rapid prototyping to production line support. Starting out as an open source project, Ultimaker was one of the first companies to make FDM printing technology accessible to the consumer. Besides developing and manufacturing 3D-printers, Ultimaker R&D is also responsible for developing the most popular 'slicing' software in the world, *Cura*. As of 2020, Cura was used a staggering 1.4 million times a week to convert digital models to physical ones. To complete the 3D-printing environment Ultimaker also offers a selection of printing materials. These materials come in ready-to-print filaments. Printing these filaments is thoroughly tested and optimized by the *print process & materials department* within Ultimaker R&D, of which I was a part during my internship. My role was expanding the Ultimaker material portfolio with a research into annealing plastics to allow the printing of stronger parts, and write an annealing guide for their interested clients: a project I thoroughly enjoyed doing.

2.1 Annealing 3D printed parts

The technique known as annealing has its origins in metallurgy. Heating up a metal to a sufficient degree followed by slow cooling, relieves the material from inner stresses causing it to become more ductile and stronger as a result. When polymers made their commercial appearance, annealing certain thermoplastics proved to be beneficial as well, and the technique was quickly adapted and implemented into the injection moulding process. Cooling down the mould after injection in a controlled way results in a stronger but - in contrast to metals that become more ductile - stiffer and more brittle product. Most notably, the material's thermal resistance (a typical weak spot of most thermoplastics) is greatly improved. The straightforward inclusion of annealing in the injection moulding process is one of the reasons injection-moulded parts out-perform 3D printed ones: once FDM printer filament leaves the nozzle, suspension in an ambient environment results in rapid cooling and an amorphous polymer structure is retained. In addition, printing semi-crystalline polymers in an amorphous state is actually preferred, even in higher-end FDM printers that employ a temperature controlled build chamber. The annealing process slightly warps the deposited polymer, causing reduced dimensional accuracy or even failed prints as the model is displaced during printing. Instead, annealing 3D-printed parts to approach the strength of injection moulding can best be done in a separate stage as illustrated in figure 1.

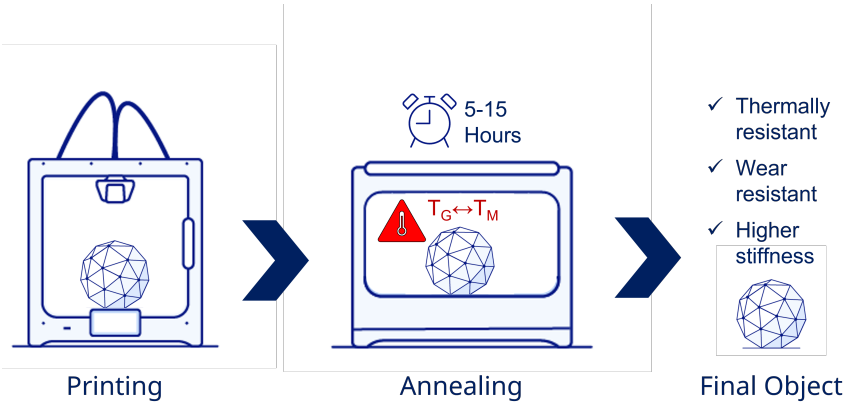

Figure 1: Annealing 3D printed parts.

2.2 The chemistry behind polymer annealing

The apparently opposite behaviour between metals becoming more ductile and polymers becoming more brittle after annealing is caused by a mechanism known as crystallization (Alejandro and Michell [2016]). In its molten state, a polymer consists of individual polymer chains that possess the freedom to flow past one another and form a flowing, amorphous mass (figure 2, on the left). When the polymer is cooled down rapidly, e.g., injected in a cold mould or extruded in an FDM printer, the amorphous composition is retained; once it passes the glass transition temperature (T_G), the amorphous state is effectively 'locked in' as the enthalpy present in the polymer is no longer enough to overcome inter-molecular forces like hydrogen bonding, polar interactions, and van der Waals forces. However, when allowed to cool down in a slow and controlled fashion to a rubbery state above T_G, the enthalpy present in the system offers the polymer chains the mobility needed to arrange themselves in energetically favorable patterns. These patterns or 'crystalline regions' are not subject to the rubbery flow of amorphous polymer and can therefore withstand temperatures above T_G without deformation, resulting in a thermally resistant material (figure 2, on the right). The re-structuring of the polymer matrix during annealing provides mechanical strength, thermal-, and chemical resistance; as such, it is the main mechanism through which annealing alters polymer properties. Because of this, only polymers able to undergo crystallization benefit from annealing - a collection restricted to the semi-crystalline group of polymers. They set themselves apart from the other group, known as amorphous polymers, by having a regular pattern of side groups that are small enough to avoid steric hindrance during the formation of crystalline regions. Polyethylene (no side groups) and Polypropylene (methyl groups) are examples of highly crystalline plastics; other forces that have a positive effect on crystallization are hydrogen bonding in nylons and aromatic interactions in polystyrene. The overview of polymers

currently used in FDM printing illustrated in figure 3 is divided between the 'annealable' semi-crystallines and fully amorphous plastics.

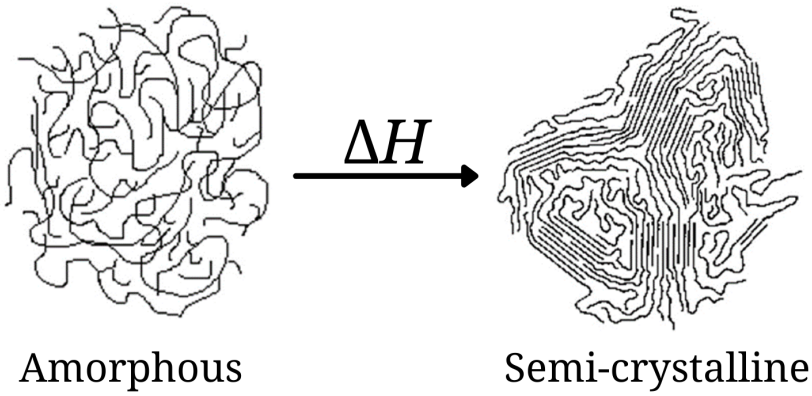

Figure 2: Heat-induced crystallization of a semi-crystalline polymer.

The two thermoplastic and semi-crystalline polymers researched in this project were PLA and carbon fiber-reinforced PET, hereafter referred to as PET-CF. PLA is a polymer of interest since it is the most common plastic used in FDM printing. It possesses great mechanical properties and is relatively easy to print, with a T_G of 60 °C and melting temperature around 190 °C. However, it lacks thermal stability in its amorphous state, and the structural integrity of 3D printed PLA parts is compromised at temperatures higher than 55 °C. As the most popular FDM printing material, improving the temperature resistance of PLA objects will have a large positive impact on the 3D printing industry as a whole. It must be said that not all PLA filaments are eligible for improvement through annealing: racemic mixtures of its *L*- and *D*-enantiomers prevent crystallization. The PLA produced by Mitsubishi Chemicals used in this research, whilst its exact composition in terms of molecular weight and *L*- and *D*-enantiomers are unknown, is semicrystalline in nature and marketed as an annealable plastic. The other plastic analyzed in this project, PET-CF, is a step up from PLA in all regards except ease of printing. the inclusion of carbon fibers offer this PET composite the stiffness of engineering-grade polymers, and annealing can offer the thermal stability it needs to compete with expensive high-performance plastics like PEEK and PEKK.

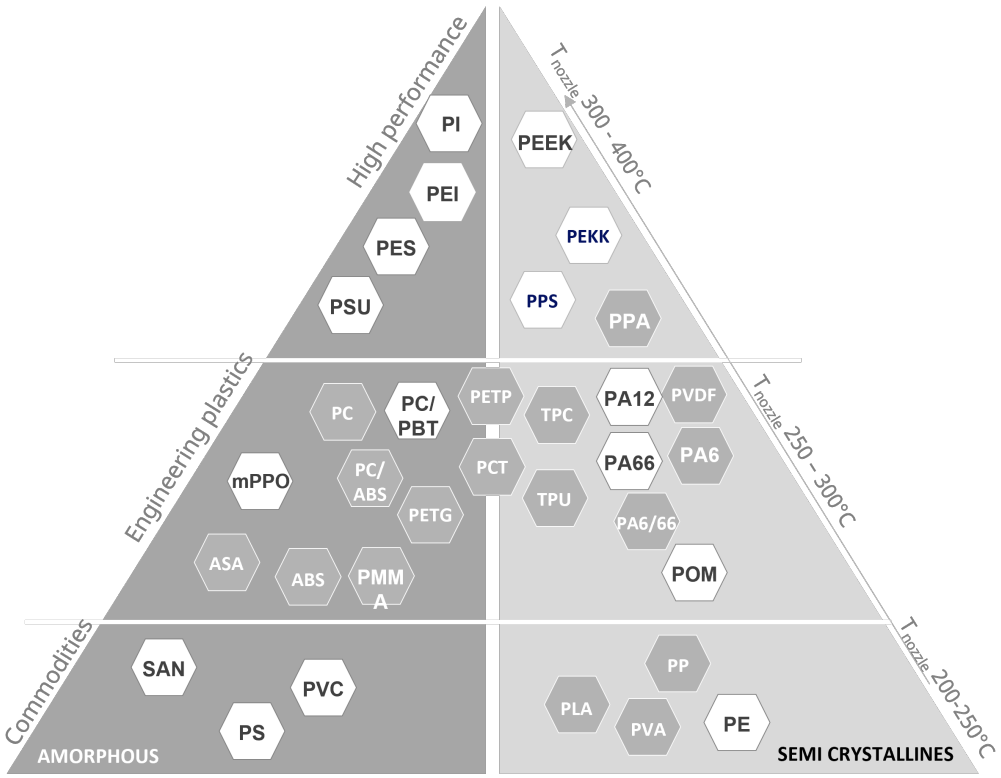

Figure 3: Overview of plastics used in FDM printing.

Annealing temperature and its effect on crystallization

Integral to this research project and the formulation of an optimal annealing workflow for prospective clients is an investigation of the influence of annealing temperature on the properties of the annealed part. As previous research has shown, polymer crystallization occurs over a range of temperatures, and crystallization mechanics change accordingly. This is illustrated in figure 4, obtained with Polarized Microscopy (PLM) Androsch et al. [2018]. Poly-*L*-lactic acid (PLLA) was crystallized at different temperatures and exhibited a starkly different distribution in *spherulites*, aggregates of crystalline regions. To understand this phenomenon, it is important to understand the formation of these spherulites in the first place. Crystalline regions do not appear spontaneously or randomly within the polymer matrix. Instead, they originate from a *nucleus*, original occurrences of crystallinity or the presence of a chemical nucleating agent. Through a chain reaction, crystallinity induces the ordering of surrounding polymer chains into crystalline structures. These crystalline 'lamellae' that grow out of these nuclei form the spherulites depicted in figure 4. The *nucleation* and *growth* of these spherulites are two competing mechanisms

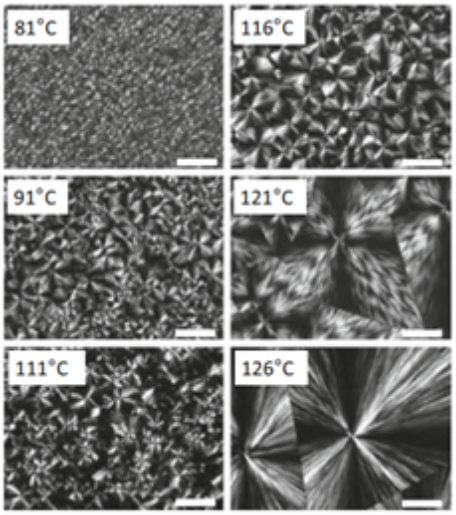

Figure 4: PLA spherulite size at different crystallization temperatures.

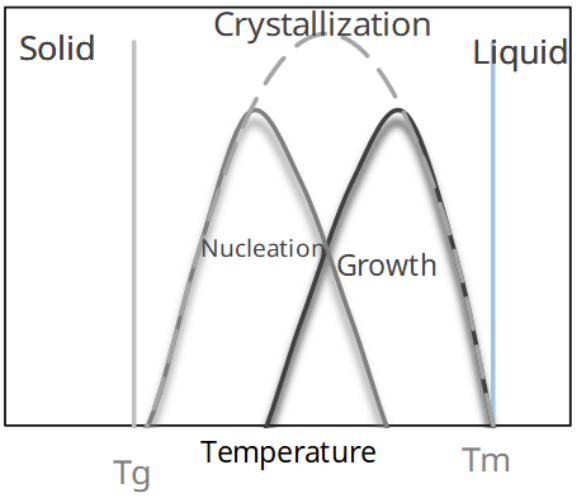

Figure 5: The two competing mechanisms of crystallization are favored at different temperatures.

that proliferate differently under the influence in temperature; low temperatures (close to T^G) seem to favor nucleation, whereas growth is promoted by higher temperatures (closer to T_M). This phenomenon is summarized graphically in figure 5. The direct consequence of this behaviour relevant to this project is that a low annealing temperature will result in a high density of smaller spherulites, as the formation of new spherulites (nucleation) is promoted over growth; conversely, high annealing temperatures result in a low density of large spherulites. The effect this difference has on the properties and warping of 3D printed parts is investigated in this project.

3 Materials

The PLA X^3 and PET-CF filaments annealed and analyzed in this research were provided by Mitsubishi Chemical Performance Polymers (MCPP) and Lehvoss (PET-CF black). Red- and black coloured filaments were used besides natural (uncoloured) PLA. PET-CF was provided in natural form (MCPP) and black (Lehvoss).

4 Methodology

PLA and PET-CF filaments were used to print samples designed for visual, mechanical and thermal property analysis. Samples were designed using *Tinkercad*, sliced using *Cura* and printed using the Ultimaker S5 FDM printer model. PLA samples were printed at 225 °C using a heated bed at 60 °C to aid bed adhesion. PET-CF samples were printed at 260 °C on an 80 °C heated bed. Different slicing orientations were evaluated. Samples were either left unannealed or annealed at varying temperatrures using a programmable industrial oven (Memmert model 1060). Annealing procedures all followed the temperature profile illustrated in figure 6. The samples were heated form room temperature to the T_G of the material and were allowed to release residual stresses for an hour before heating to the chosen annealing temperature to crystallize over a timespan of two hours. Destressing- and annealing periods at T_G and the chosen T_C respectively were kept constant, as were the temperature ramps for heating and cooling. To determine appropriate annealing temperatures, the exothermic process of crystallization for both PLA and PET-CF was monitored using Differential Scanning Calorimetry (DSC). PLA appeared to crystallize between 80 and 110 °C; low-temperature annealing was therefore performed at 80 °C, high-temperature annealing at 110 °C. PET-CF exhibited a wider crystallization range (120-220 °C) and therefore 3 annealing temperatures were decided upon: 120, 170, and 220 °C.

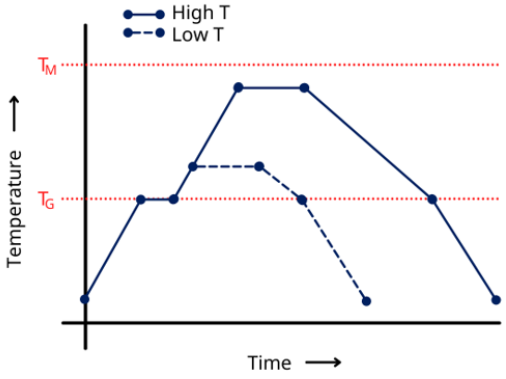

Figure 6: Annealing temperature profiles.

4.1 Degree of crystallinity

Changes in sample crystallinity before- and after annealing were measured using the Linseis chip-DSC 10 instrument. DSC samples were removed from the top of the 100 mm tripod model designed for shrinkage and warping analysis to avoid the measurement of crystallization induced by the heated bed of the printer, which would be present near the base of the model. Samples endured two melting cycles from 30 °C to 230 °C (PLA) to 300 °C (PET-CF). An example of DLC analysis of unannealed PET-CF is depicted in figure 8. Of interest are the (exothermic) peaks of crystallization (±120-150 °C) and re-crystallization (±200-220 °C), and the endothermic valley associated with melting at ±240-270 °C. Integration of these peaks yields the energy either released (in exothermic processes) or absorbed (in endothermic processes). The melting enthalpy of a given polymer is for a large part determined by its crystallinity: 100% amorphous polymers exhibit

no clear phase change from an amorphous solid to an amorphous rubber and finally to an amorphous liquid when temperature is increased.

However, crystallinity is not fully accountable for the melting enthalpy. The contribution of the sample's original crystallinity to its melting enthalpy was determined in two ways: first, any enthalpy of crystallization that occurred prior to melting (only the case in unnannealed samples, figure 8a) was subtracted from the melting enthalpy. Second, the contribution of crystallinity to the melting enthalpy was determined by comparing the recrystallization peak of the first cycle (23.4 J/g for the unannealed example) to the melting enthalpy in the second cycle (-11.1 J/g). The fact that the second melting enthalpy is lower than the re-crystallization that came before it implies a loss of crystallinity-related enthalpy somewhere. This was the case for all PET-CF samples, whereas PLA exhibited the opposite with larger melting peaks than recrystallization peaks. Both phenomena were accounted for by subtracting this difference between known crystallinity and observed melting enthalpy from the original melting enthalpy in the first cycle. This was a rather rough approximation of the 'true' amount of enthalpy contributed bythe sample's crystallity, but deemed accurate enough given the analytical methods that were at hand; It was more accurate than taking the melting enthalpy at face value and good enough for comparisons between different annealing methods of the materials studied in this project. With the melting enthalpy that was thus obtained, sample crystallinity could be determined by comparison with theoretical melting enthalpies of 100% crystalline polymers found in literature: 93 J/g for PLA [Lim, L. T., et al., 2008; Avérous, L., 2008], 140 J/g for PET, using equation 1:

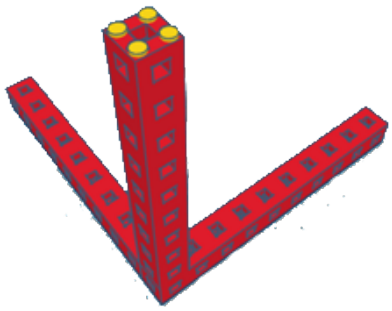

Figure 7: Digital model of the tripod designed for visual and warping analysis (red) including protrusions for DSC testing (yellow).

$$\text{Crystallinity}\% = \frac{|\Delta H_{m,1}| - |\Delta H_c| - (|\Delta H_{rc}| - |\Delta H_{m,2}|)}{|\Delta H_{c,100\%}|} \cdot 100\% \tag{1}$$

With:

$\Delta H_{m,1}$	= Enthalpy of melting, first cycle
ΔH_c	= Enthalpy of crystallization
ΔH_{rc}	= Enthalpy of recrystallization, first cycle
$\Delta H_{m,2}$	= Enthalpy of melting, second cycle
$\Delta H_{c,100\%}$	= Theorhetical enthalpy of melting 100% crystalline polymer

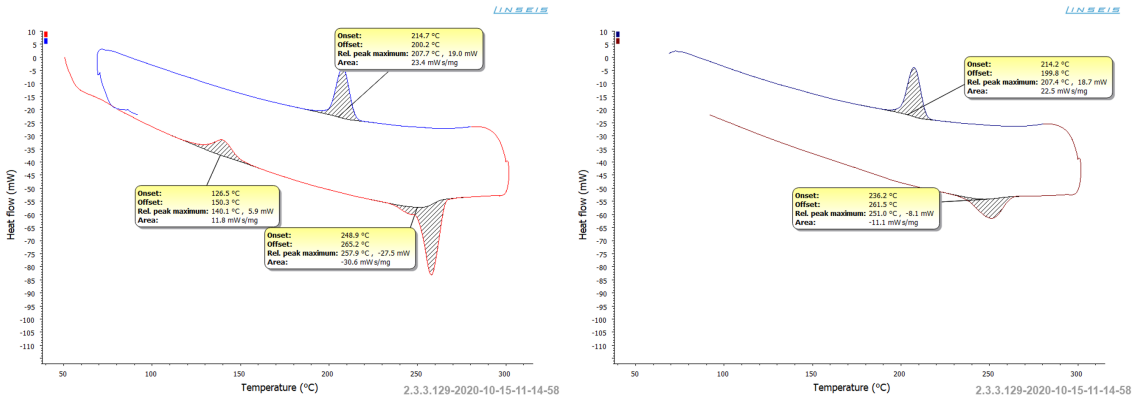

(a) Unannealed PET-CF

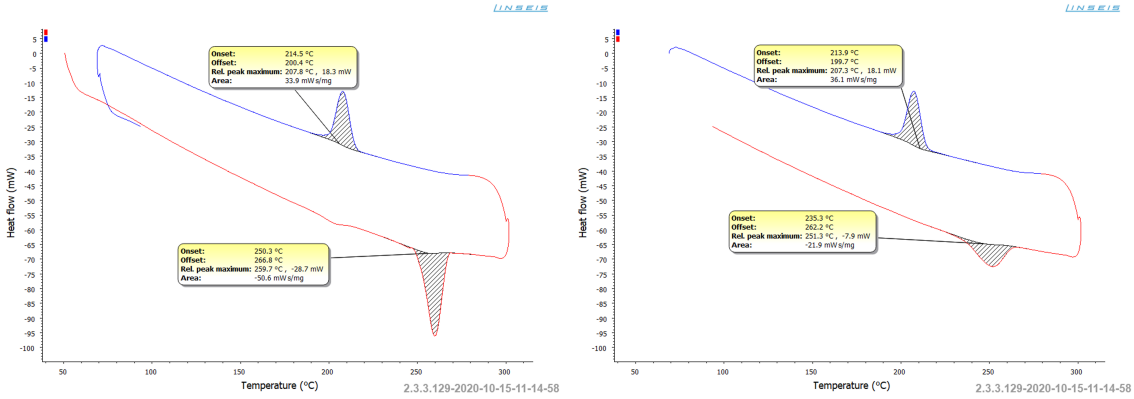

(b) Annealed PET-CF (170 °C)

Figure 8: Heating (red) and cooling (blue) cycles of both unannealed and annealed PET-CF measured using DSC.

4.2 Part shrinkage and warping

Due to a more efficient packing of polymer molecules in crystalline structures compared to their amorphous counterparts, a certain degree of shrinkage after annealing is to be expected. In addition, as annealing takes place above the T_G, rubbery flow can cause further warping of the 3D object. Both shrinkage and warping were analyzed using the tripod discussed in 4.1. All arms of this tripod, designed to be 100 mm along x, y, and z axes, were measured using a set of calipers before and after annealing (figure 9a. The tripods were also visually analyzed for warping (9b and 9c). All tripods were annealed and measured in duplo. Finally, a puzzle piece and -slot were designed in such a way that only a sample printed at 100% size could fit. When printed at 99% (simulating a shrinkage of the material of 1%) it would not fit anymore (figure 9d). This puzzle piece was annealed

and its fit was evaluated for every material and annealing temperature.

(a)

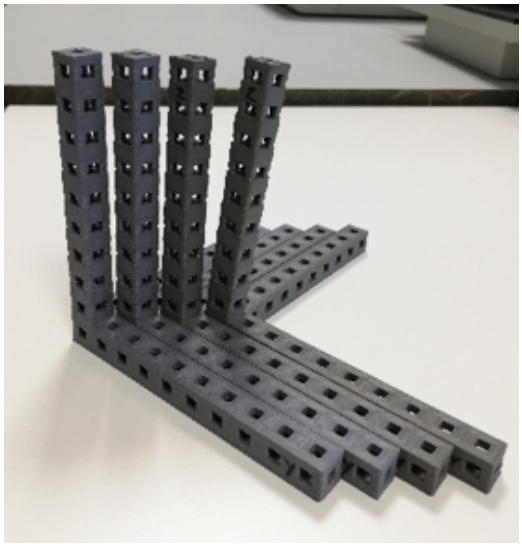

(b)

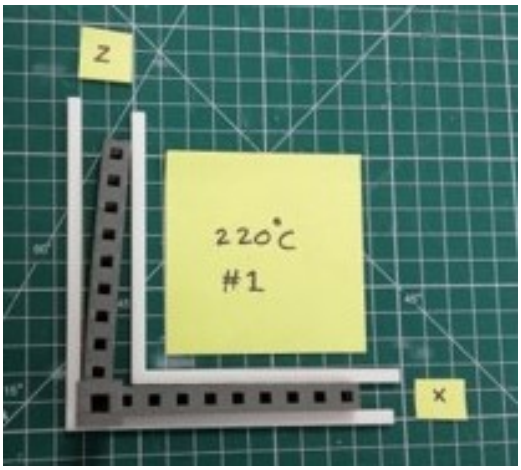

(c)

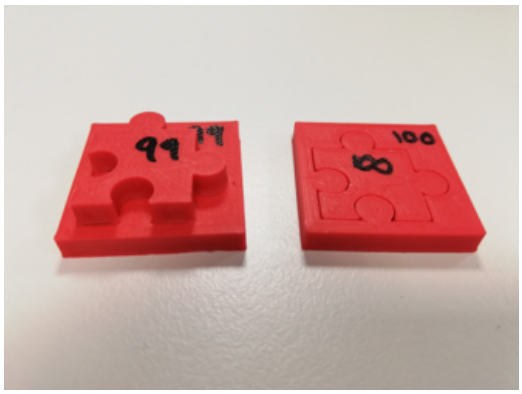

(d)

Figure 9: Measuring object shrinkage (a), visual analysis of warping (b)&(c), and a qualitative analysis of shrinkage (d).

4.3 Mechanical properties

Flexural stiffness and strength were measured using the Instron 3366 universal testing system according to industry standard ISO 178. In the ISO 178 flexural test, bars are subjected to a variable stress needed to obtain a steady rate of deformation or strain, producing the modulus (stiffness) and the maximum stress before plastic deformation (strength). Because properties of 3D printed parts are inherently anisotropic due to the layer-by-layer nature of FDM printing, flexural testing bars measuring 80x10x4 mm were printed flat (XY) and standing upright (Z). XY-printed samples were used to test resistance to forces parallel to print direction, Z-printed samples for forces perpendicular to print direction (effectively testing Z-layer adhesion of the sample). The effects of annealing in this regard are largely unknown, as layer lines are not present in conventional methods of fabrication, like injection-moulding.

Figure 10: A flexural test using red PLA.

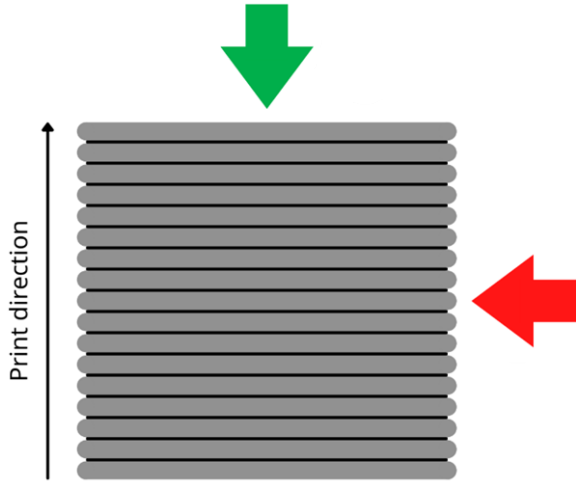

Figure 11: XY-printed samples test forces from above (green); Z-printed samples test forces from the side (red).

4.4 Thermal properties

Analysis of thermal properties was performed externally at MCPP Netherlands BV, the supplier of both PLA X^3 and PET-CF. XY Flexural bars of 80x10x4 mm were printed and annealed together with the flexural samples described in section 4.3 before being sent to MCPP Netherlands, where the Heat Deflection Temperature (HDT) was determined using the HDT-A method outlined in industrial standard ISO-75. This test is similar to the flexural test, but handles a constant load whilst the sample is submersed in an oil bath that is hetaed by 2 °C per second (figure 12). The temperature at which the deformation or strain reaches 0.35 mm is recorded as HDT. The HDT-A method handles an outer fibre stress of 1.82 MPa (as opposed to 0.455 MPa used for HDT-B).

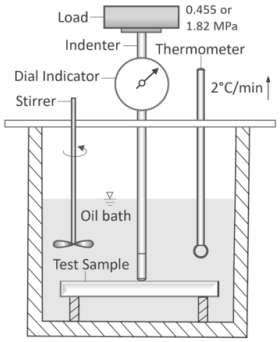

Figure 12: HDT set-up.

5 Results and discussion

This section presents the results obtained in this project. It is structured as follows: first, general observations and good practices regarding annealing will be provided; Then, the effects of annealing on the properties of PLA are presented, followed by the effects on PET-CF.

5.1 Annealing method

As an initial test to determine whether object placement had an effect on warping, three PLA tripods were annealed at 110 °C whilst each had a different arm oriented upwards (x and y arms upwards meant placement at a 90° angle, whereas z arm upwards maintained print orientation). The results are depicted in figure 13. While warping was minimal in all cases, the best results were obtained when print orientation was maintained during annealing.

A follow-up investigation into the effect of model infill (the degree to which the part was filled with polymer as opposed to hollow, determined pre-slicing) on warping was recorded by printing XY- and Z-flexural bars at either 100% or 0% infill prior to annealing at 110 °C. All bars where annealed in XY orientation, meaning XY-printed bars remtained print orientation whereas Z-printed bars were annealed under a 90° angle. As can be observed in figure 14 XY printed bars at 100% infill produced the best results, whereas Z printed bars at 0% exhibited high levels of warping.

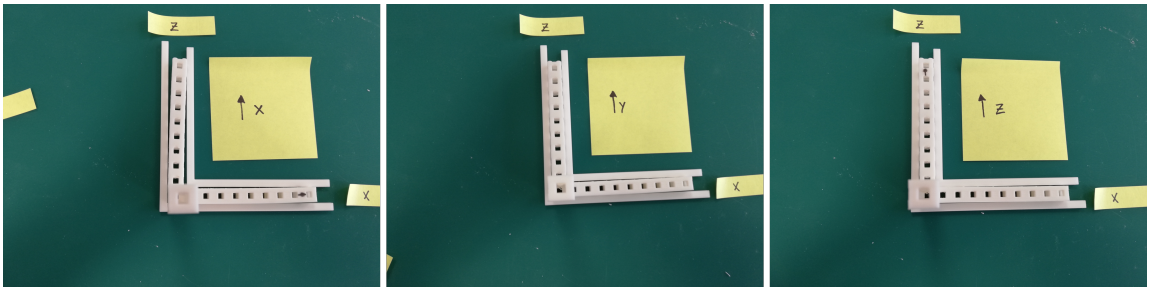

Figure 13: maintaining object print orientation during annealing minimizes warping. F.L.T.R.: annealed with x-, y-, and z printing directions upwards.

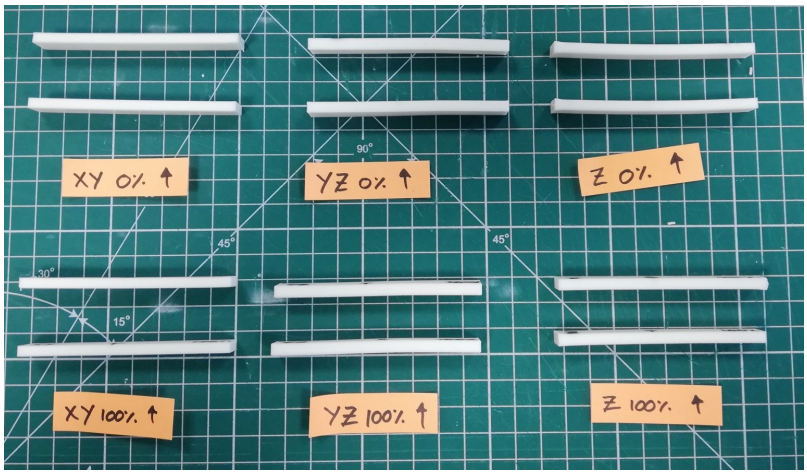

Figure 14: Higher infill levels inhibited warping.

5.2 Annealing PLA X^3

This section covers the results of annealing PLA X^3 in the folllowing order: shrinkage and warping, degree of crystallization, mechanical properties and thermal properties. For an overview of all these results, please consult the appendix (page 29)

Shrinkage and warping

PLA X^3 exhibited minimal shrinkage and warping. The shrinkage recorded by tripod measurements before and after annealing can be found in table 1. In essence, shrinkage in all directions remained below 1% for all annealing temperatures, and consequentially puzzle pieces remained a snug fit as well. Likewise, warping was negligible when print orientation was maintained during annealing (figure 13.

Axis	1	2	Avg.
x	-0.7%	-0.4%	-0.6%
y	-0.9%	-0.0%	-0.4%
z	0.1%	-0.2%	-0.1%

80 °C

Axis	1	2	Avg.
x	-0.6%	-0.4%	-0.5%
y	-0.6%	-0.5%	-0.6%
z	-0.4%	-0.3%	-0.4%

110 °C

Table 1: Recorded shrinkage at different annealing temperatures.

Degree of crystallinity

The crystallinities determined according to the procedure outlined in section 4.1 are recorded in table 2. A clear increase in crystallinity is observed after annealing, but annealing temperature seems to have no further effect as both low- and high- temperature annealing yielded similar crystallinities. This not only indicates that full potential crystallinity has been achieved in both cases, as the annealing procedure of 110 °C takes three hours longer, it also implies that any changes in properties between annealing methods were due to a different organization of crystalline regions as illustrated on page 7. The spread for each crystallinity, derived from three separate samples sourced from two tripod models, was also minimal, making any claims regarding crystallinity more convincing. Unannealed, PLA X^3 already seems to be on the higher end of the crystallinity spectrum: PLA usually has a crystallinity lower than 10%. The 30% crystallinity obtained after annealing is significant; a crystallinity of 66%, considered the highest PLA crystallinity recorded, was obtained after optimized high-temperature and high-pressure conditions (Zhang et al. [2012]).

Annealing T	Crystallinity	Deviation
Unannealed	9%	±1%
80 °C	30%	±2%
110 °C	29%	±1%

Table 2: Crystallinity of PLA X^3 after annealing.

Mechanical properties

Annealing directly influenced the behaviour of samples that endured flexural testing, as shown by the photographs in figure 15. Unannealed samples bent where the more brittle annealed samples (partially) broke: a clear indication of an increase in brittleness. Wider tears, indicative of higher brittleness, are found in samples annealed at 110 °C.
Like brittleness, stiffness increased with annealing temperature (figure 23), with samples annealed at 120 °having the highest flexural modulus - although the difference is small (5.2%). Flexural strength also increased after annealing, but experienced an optimum (+10.7%) at low temperature annealing (80 °C).

(a) (b) (c)

Figure 15: Flexural bars after testing: unannealed (a), 80 °C (b), and 120 °C (c).

In contrast to the XY stiffness and strength, Z-adhesion deteriorated after annealing. The flexural results can be observed in figure 17 Both the stiffness of Z samples and their strength decreased; markedly, samples annealed at low temperatures suffered the most (Modulus: -5.6%, strength: -19.2%). It seems that instead of rubbery flow enhancing inter-layer contact, shear induced by the individual shrinkage of layers builds stresses along the Z-axis. In order to investigate whether the annealing orientation had an impact on Z-layer adhesion (Z-printed samples were annealed flat like their XY counterparts) a specially designed support was printed (figure 18)

Thermal properties

Heat deformation analysis performed by MCPP yielded the values listed in table 3. The HDT values of 64 °C and 67 °C after annealing (an increase of ±10 °C seemed) seemed rather low compared to earlier PLA X^3 annealing research by Ultimaker R&D that employed the HDT-A method (118 °C). To understand exactly what these temperatures say about the thermal resistance of PLA X^3, it is important to understand what is being measured. HDT-A and HDT-B are identical procedures, except for a higher stress applied in HDT-A (1.8 MPa vs 0.455 MPa, page 4.4). As a result, the required deformation of 0.34 mm occurs earlier and a lower HDT is recorded. It is worth to note that both methods were developed in the 1970's (Zweben et al. [1979]) when plastics were not as highly developed, and set an accordingly low standard with respect to polymer applications today. Both loads are small (3N for HDT-A and 0.76N for HDT-B), and deformation occurs within minutes, therefore the usability of a part at elevated temperatures, higher loads and over larger time-spans requires consideration beyond HDT.
The HDT effectively measures at what temperature the sample has softened to such a

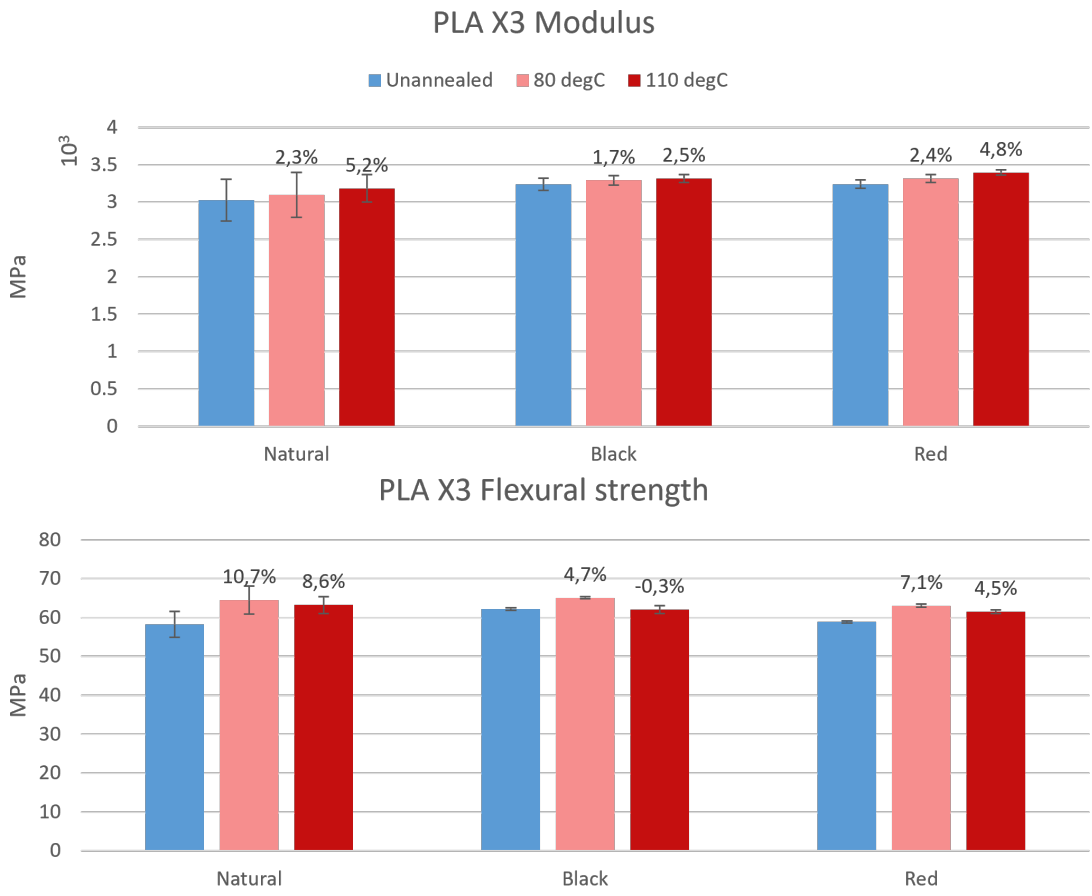

Figure 16: Flexural modulus and strength of PLA X^3.

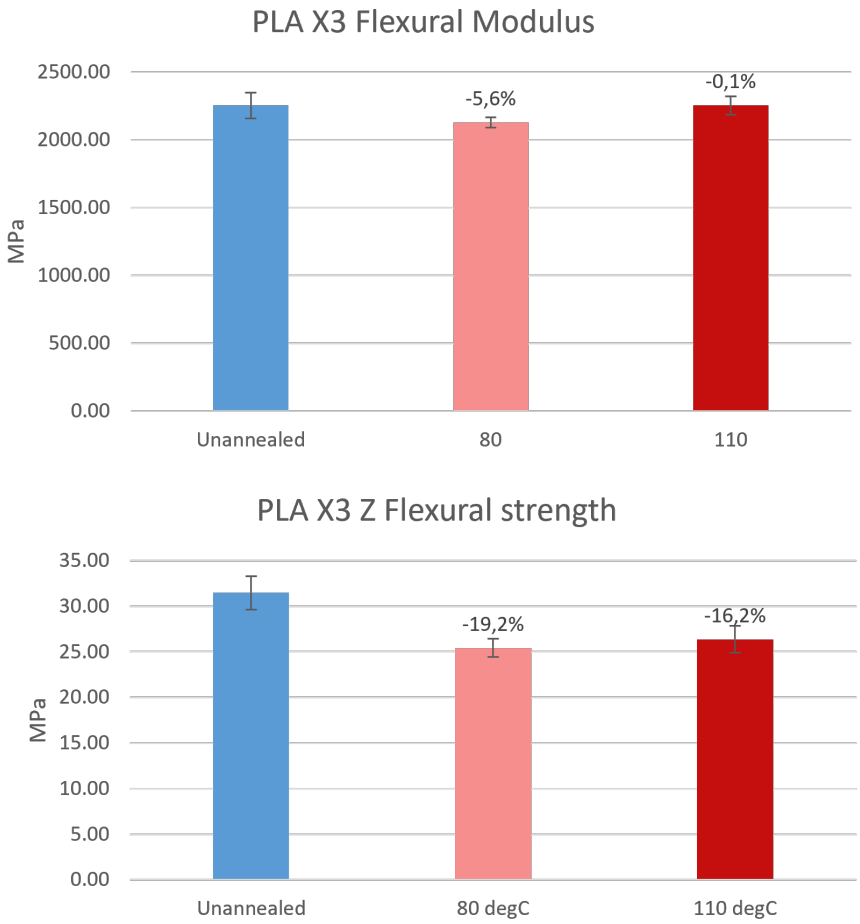

Figure 17: Flexural modulus and strength of PLA X^3 (Z-direction).

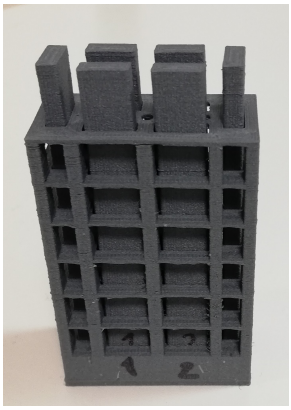

Figure 18: Holder for maintaining Z-sample print orientation during annealing.

Annealing temperature	HDT-A	HDT-B
Unannealed	54 °C	57 °C
80 °C	64 °C	
110 °C	67 °C	118 °C

Table 3: HDT-A data as received from MCPP and HDT-B data from previous research.

degree that the applied force is enough to overcome the flexural modulus of the material, and the sample is bent 0.32 mm. In an attempt to visualize the thermal behaviour of PLA X^3, a sketch was produced (figure 19) that incorporated both HDT-A data from MCPP and HDT-B data. The moduli that correspond to the HDT A and HDT B were calculated using equation 2, after calculating the load (F) using equation 3 from elastic beam theory.

$$E_{\text{flex}} = \frac{L^3}{wh^3\delta}F \tag{2}$$

$$F = \frac{2E_{\text{flex}}wh^2}{3L} \tag{3}$$

With:

ΔE_{flex}	= Flexural modulus, in MPa
L	= Sample length between supports, in mm
w	= Sample width, in mm
h	= Sample thickness, in mm
δ	= Sample deformation, in mm
F	= Load, in N

Figure 19 was sketched using principles of literature (Alejandro and Michell [2016]), the moduli determined using flexural testing (see figure 23), and the HDT data of table 3. Around T_G, the amorphous regions lose their stiffness. For highly amorphous polymers, this means a total loss of structural integrity, as exemplified by the unannealed PLA X^3 having similar values for both HDT-A and HDT-B. However, semicrystalline polymers can rely on their crystalline regions for stiffness beyond T_G. A significant drop around T_G is still to be expected as the amorphous regions lose their stiffness. In the greaph, moduli were plotted as constants before T_G, dropped at T_G until they bisected a straight line plotted through HDT-A and HDT-B values (unannealed and 110°C, extrapolated for 80 °C) that represented the modulus of the crystalline regions.

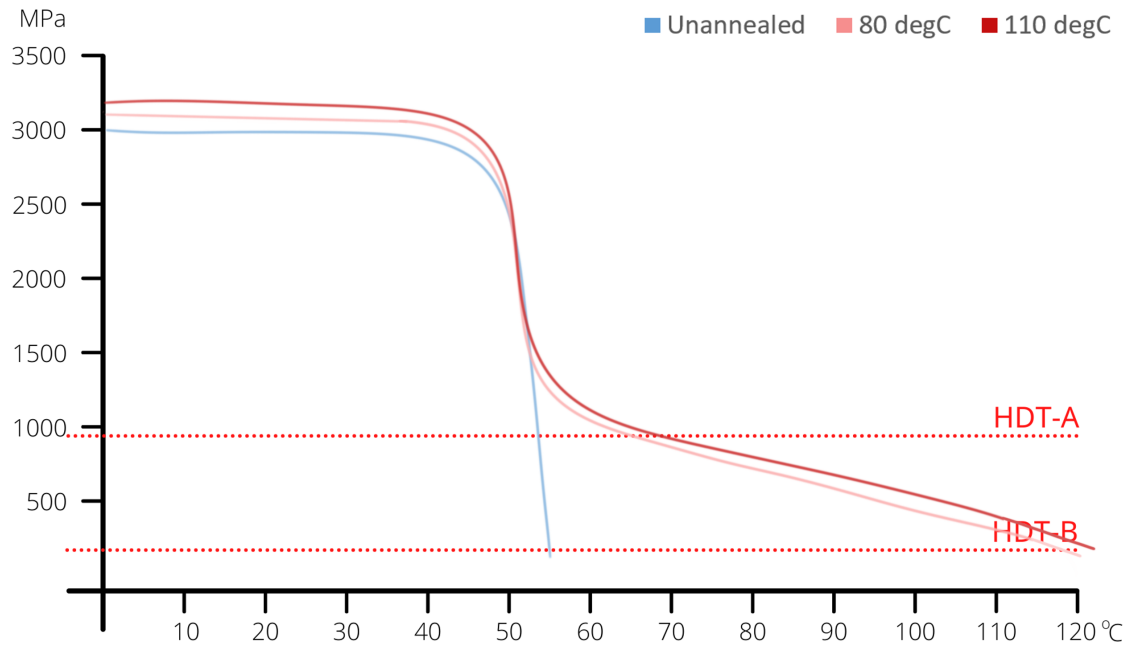

Figure 19: A rough sketch of thermal behaviour of PLA X^3. Flexural modulus as a function of temperature.

Figure 19 indicates that annealing PLA has a large impact on its thermal resistance, and the material can be used at temperatures higher than the T_G of 60 °C for purposes that do not involve heavy loads. The difference between annealing temperatures seems marginal.

5.3 Annealing PET-CF

This section covers the results of annealing PLA X^3 in the folllowing order: shrinkage and warping, degree of crystallization, mechanical properties and thermal properties. For an overview of all these results, please consult the appendix (page 29). Unlike PLA X^3,

which exhibited no discernible visual change upon annealing, PET-CF showed signs of degradation after annealing at 220 °C. The yellow tint, visible in figure 20, was only present at the surface. This discoloration indicates oxidation of the polymer surface, a closer inspection of the cross-section indicates that the bulk volume was untouched.

(a) (b) (c)

Figure 20: PET-CF after annealing: regular color after 120 °C (a), discoloration after 220 °C (b), Cross-section after 220 °C (c).

Shrinkage and warping

Like PLA X^3, PET-CF exhibited minimal shrinkage and warping for annealing temperatures up to 170 °C. The shrinkage recorded by tripod measurements before and after annealing can be found in table 4. Shrinkage remained mostly below 1%. Z direction shrinkage proved to be larger than in x and y directions, shrinking more than 2% after annealing at 220 °C. As was the case with PLA X^3, all puzzle pieces provided a snug fit before and after annealing. Like shrinkage, warping was more pronounced after 220 °C annealing (figure 9b)

Degree of crystallinity

The crystallinities determined according to the procedure outlined in section 4.1 are recorded in table 5. As with PLA, a clear increase in crystallinity is observed after annealing, and low-medium annealing temperature seems to have no further effect. However, high temperature annealing (220 °C) produced a crystallinity of 36%. This apparent oddity can be explained by the degradation of the sample surface highlighted on page 5.3, which certainly would have an effect on the small sample located on said surface. Oxidation of this DLC

Axis	1	2	Avg.
x	-0.6%	-0.6%	-0.6%
y	-0.6%	-0.6%	-0.6%
z	-0.9%	-1.0%	-0.9%

120 °C

Axis	1	2	Avg.
x	-0.7%	-0.8%	-0.8%
y	-0.8%	-0.8%	-0.8%
z	-2.0%	-2.2%	-2.1%

220 °C

Axis	1	2	Avg.
x	-0.6%	-0.6%	-0.6%
y	-0.6%	-0.7%	-0.6%
z	-1.2%	-1.2%	-1.2%

170 °C

Table 4: Recorded shrinkage at different annealing temperatures.

sample may have led to a myriad of chemical alteration and even crosslinks, that would significantly increase the enthalpy of melting. The rather large spread (±10%) supports the notion of a variable chemical composition as a result of degradation. The crystallinity of annealed PET-CF seems low in comparison to industrially annealed PET, which falls in a range of 30-60% (Aharoni et al. [1983]); A reason could be the presence of carbon fibres, but the material has not been specifically marketed for annealing (unlike PLA X^3) and is thus unlikely to be optimized for this purpose.

Annealing T	Crystallinity	Deviation
Unannealed	8%	±3%
120 °C	22%	±2%
170 °C	20%	±4%
220 °C	36%*	±10%

Table 5: Crystallinity of PET-CF after annealing.
*Value likely distorted by degradation.

Mechanical properties

Like PLA X^3, PET-CF brittleness increased after annealing. As depicted in figure 22, unannealed PET-CF broke partially, but all annealed samples broke completely under enough stress. Flexural stiffness and strength also followed the same trend found in PLA X^3, even more pronounced: Higher annealing temperatures resulted in stiffer, but weaker samples compared to low annealing temperatures. However, one large difference stands out: where PLA X^3 all annealed samples were stronger than their unannealed version, PET-CF annealed at 220 °C actually decreased in strength (-12,9%). Contrastingly, PET-CF annealed at 120 °C resulted in a flexural strength increase of 16.9%.

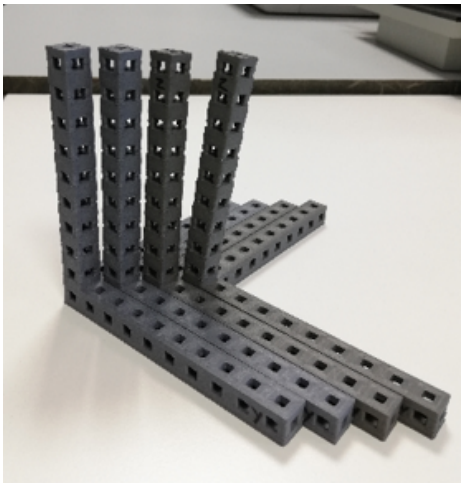

(a)

(b)

Figure 21: Warping was more pronounced at 220 °C. F.L.T.R.: 120 °C, 170 °C 220 °C, 220 °C (a). Regardless of annealing temperature, puzzle pieces still fit (b)

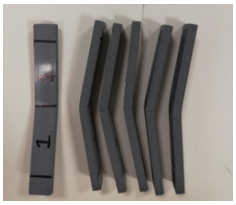

(a)

(b)

(c)

(d)

Figure 22: Flexural bars after testing: unannealed (a), 120 °C (b), 170 °C (c), and 220 °C (d).

In another parallel to PLA X^3, Z-adhesion deteriorated after annealing PET-CF as well. Despite becoming significantly stiffer (modulus +33%) flexural strength decreased (-31.7%) when samples were annealed at 220 °C. It is possible that oxidation increases the detriment to Z-layer adhesion and one of the reasons this decrease in strength is this extreme. 120 °C annealing resulted in a less significant decrease of -13.2%.

Thermal properties

Using the same method described previously for PLA, a sketch of the thermal behaviour of PET-CF (figure 25) was created using the data collected from MCPP and previous research by Ultimaker R&D (table 6). In contrast to PLA X^3, annealing temperature seemed to have a dramatic effect the temperature resistance of PET-CF, with an incredible HDT-A

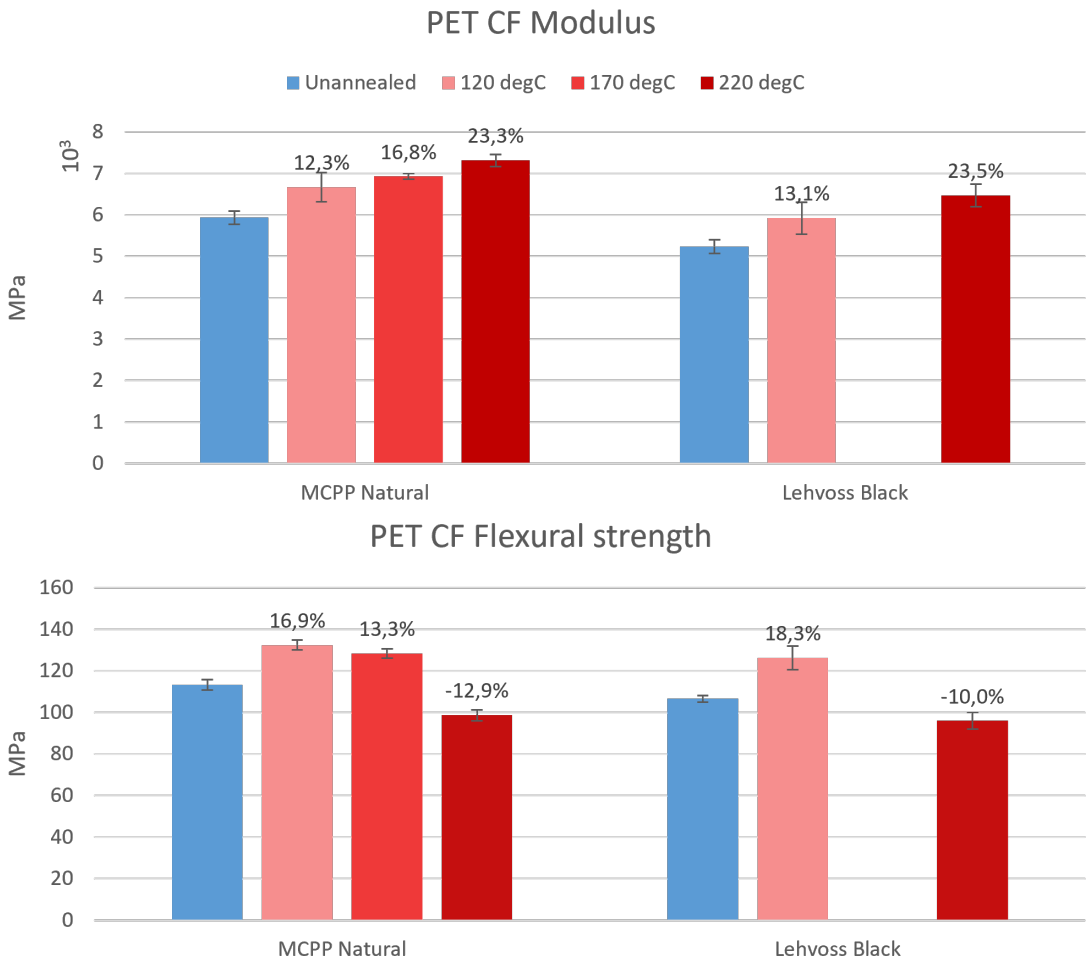

Figure 23: Flexural modulus and strength of PET-CF.

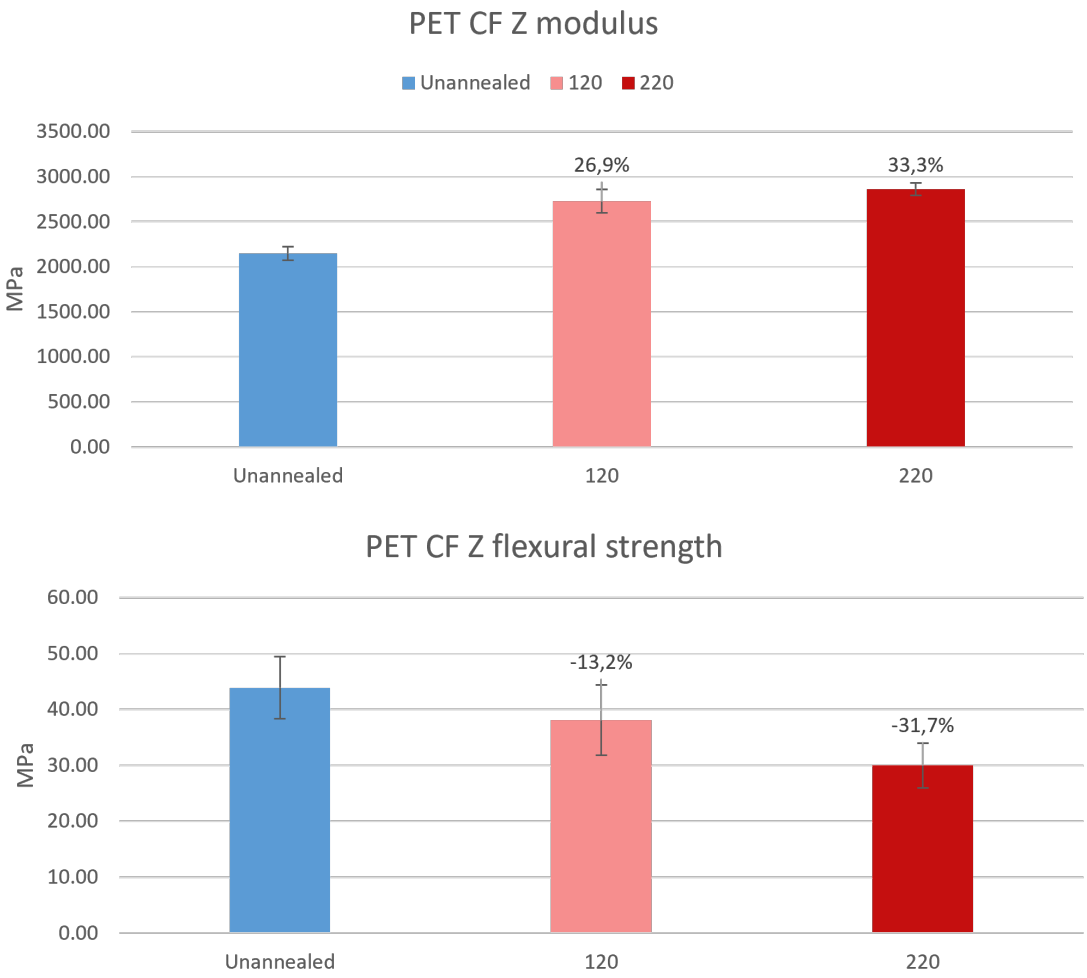

Figure 24: Flexural modulus and strength of PET-CF (Z-direction).

increase of 74 °C (unannealed) to 229 °C (220 °C annealing). In a striking pattern, HDT-A was equal to the annealing temperature + 10 °C. Figure 25 indicates that not only is the HDT higher for samples annealed at a higher temperature, their stiffness also significantly increased beyond T_G compared to lower annealing temperatures.

Annealing temperature	HDT-A	HDT-B
Unannealed	74 °C	79 °C
120 °C	130 °C	183 °C
170 °C	182 °C	
220 °C	229 °C	

Table 6: PET-CF HDT-A data as received from MCPP and HDT-B data from previous research.

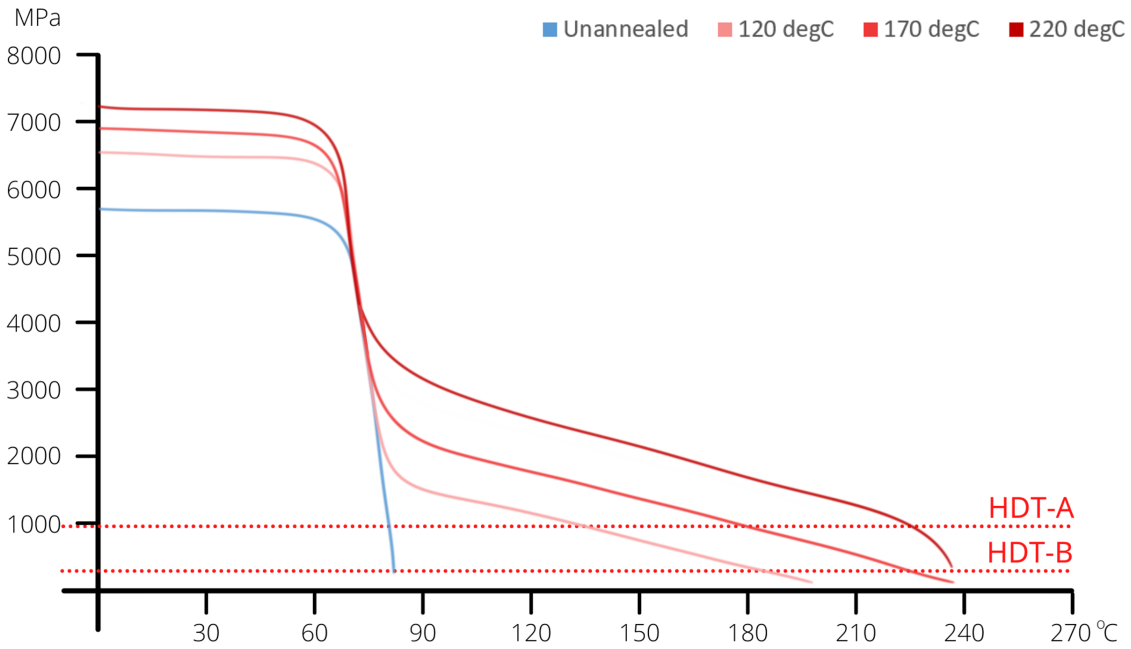

Figure 25: A rough sketch of thermal behaviour of PET-CF. Plotted are the modulus as a function of temperature.

6 Conclusion

When done right, annealing 3D printed parts of PLA X^3 and PET-CF causes minimal shrinkage or warping, but can have a large impact on mechanical and thermal properties. Flexural strength and stiffness can be improved as well as thermal resistance past the material's T_G by applying the right annealing procedure. Different annealing temperatures have their own benefits and drawbacks, making it important to keep the specifications of the final product in mind. Low temperature annealing promotes higher flexural strength PET-CF was 18.5% stronger when annealed at 120 °C), whereas high temperature annealing induces a higher temperature resistance instead. For PLA X^3 the latter difference between annealing procedures is all but negligible, but the thermal resistance of PET-CF improves greatly with annealing temperature: between the annealing range of 120-220 °C, HDT increased from 74 (unannealed) to a 130 °C, 182 °C and 229 °C for samples annealed at 120 °C, 170 °C, and 220 °C respectively. In contrast to flexural strength, Z-layer adhesion decreased after all annealing procedures, with high-temperature annealing of PET-CF suffering the most. Shrinkage remained constantly below -1%. Warping was minimal but print quality deteriorated slightly at higher annealing temperatures, with PETCF exhibiting signs of surface oxidation after annealing at 220 °C. Considering all effects of annealing temperature on mechanical, thermal and print quality properties, a good rule of thumb is to select an annealing temperature that is as low as possible but provides enough thermal stability for the purpose of the annealed part. The modulus-temperature sketches produced in this project provide a reference for this purpose, but further research can be done to refine these estimations of polymer stiffness at elevated temperatures, and prolonged use.

References

J. Müller Alejandro and Rose Mary Michell. *Morphology Polymer*. 2016. ISBN 9781118452158.

René Androsch, Christoph Schick, and Maria Laura Di Lorenzo. Kinetics of Nucleation and Growth of Crystals of Poly(l-lactic acid). In Maria Laura Di Lorenzo and René Androsch, editors, *Synthesis, Structure and Properties of Poly(lactic acid)*, pages 235–272. Springer International Publishing, Cham, 2018. ISBN 978-3-319-64230-7. doi: 10.1007/12_2016_13. URL https://doi.org/10.1007/12$_2$016$_1$3.

Jin Zhang, Ding Xiang Yan, Jia Zhuang Xu, Hua Dong Huang, Jun Lei, and Zhong Ming Li. Highly crystallized poly (lactic acid) under high pressure. *AIP Advances*, 2(4), 2012. ISSN 21583226. doi: 10.1063/1.4769351.

S. M. Aharoni, R. K. Sharma, J. S. Szobota, and D. A. Vernick. Crystallinity of pure and nucleated PET. *Journal of Applied Polymer Science*, 28(7):2177–2186, 1983. ISSN 10974628. doi: 10.1002/app.1983.070280705.

Annealing result overview PLA X³ and PET-CF.

PLA X3		XY Modulus		XY Stress		Crystallinity	Z Modulus		Z Stress		Thermal resistance XY		Thermal resistance Z		Shrinkage	
Colour	Temp. (°C)	Avg. (Mpa)	Increase	Max. (Mpa)	Increase	Avg.	Avg. (Mpa)	Increase	Max. (Mpa)	Increase	HDT (°C)	Increase (°C)	HDT (°C)	Increase (°C)	x	y	z
Natural	Unannealed	3026		58		9%	2256		31		56		54				
	80	3097	2.3%	65	10.7%	30%	2129	-5.6%	25	-19.2%	64	0	64	0	-0.6%	-0.2%	-0.1%
	110	3184	5.2%	63	8.6%	29%	2255	-0.1%	26	-16.2%	67	2	64	0	-0.4%	-0.6%	-0.3%
Black	Unannealed	3238		62													
	80	3292	1.7%	65	4.7%										-0.6%	-0.4%	-0.1%
	110	3318	2.5%	62	-0.3%										-0.5%	-0.6%	-0.4%
Red	Unannealed	3240		59													
	80	3318	2.4%	63	7.1%												
	110	3395	4.8%	62	4.5%												

PET CF		XY Modulus		XY Stress		Crystallinity	Z Modulus		Z Stress		Thermal resistance XY		Shrinkage		
Colour	Temp. (°C)	Avg. (Mpa)	Increase	Max. (Mpa)	Increase		Avg. (Mpa)	Increase	Max. (Mpa)	Increase	HDT (°C)	Increase (°C)	x	y	z
MCPP Natural	Unannealed	5933		113		8%	2149		44		74				
	120	6664	12.3%	132	16.9%	22%	2728	27%	38	-13%	130	56	-0.6%	-0.6%	-0.9%
	170	6928	16.8%	128	13.3%	20%					182	108	-0.6%	-0.6%	-1.2%
	220	7315	23.3%	99	-12.9%	36%	2863	33%	30	-32%	229	155	-0.8%	-0.8%	-2.1%
Lehvoss Black	Unannealed	5237		107											
	120	5921	13.1%	126	18.3%										
	220	6469	23.5%	96	-10.0%										